

# NUMERICAL INVESTIGATION OF TOOL-PART INTERACTIONS IN COMPOSITES MANUFACTURING

Ö. Özgü Özsoy\*, Nuri Ersoy\*, Michael R. Wisnom\*\*  
 \*Bogazici University, \*\*University of Bristol

**Keywords:** *composites, modelling, spring-in, tool-part interaction, warpage, manufacturing*

## Abstract

In this study, models for flat strips, and C- and L- section parts made of fibre reinforced composites are developed to investigate shape distortions, and stress distributions built up during manufacturing. The models developed capture most phenomena observed in composite parts such as corner thickening, spring-in, and arm-bowing.

## 1 Introduction

Sources of manufacturing distortions in composite manufacturing and their relative contributions to the final shape of the composite parts have attracted considerable research effort. The resulting distorted shapes consistently show a convex up curvature as the middle of the flat symmetric part lifts away from the tool. A number of parameters were found to affect the measured warpage in flat sections, the most prominent being the mismatch of coefficient of thermal expansions (CTE) between the tooling and the component [1]. Other factors are through-the-thickness fibre volume fraction gradients, lay-up orientation, part thickness and shape, use of release agent/film and the cure cycle [2, 3].

When the laminate is laid on a tool that has a considerably higher CTE and the consolidation pressure is applied, a shear interaction develops at the tool-part interface during the temperature ramps of the Manufacturer's Recommended Cure Cycle (MRCC), putting the tows close to the tool surface in tension. This occurs at the early stages of the cure, before the resin cures, when the resin modulus is low, causing a decay of tensile stresses away from the tool surface. This stress profile is locked in as the cure completes and when the part is removed from the tool, the locked in stresses cause a bending moment, forcing the part to warp in a concave-up sense (Fig. 1).

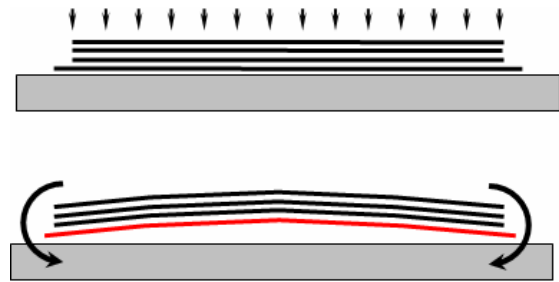


Fig. 1. Warping of flat laminates due to tool interaction

Other researchers emphasised the effect of tool-part interaction on spring-in [4-7], all agreeing that the tool interaction causes an increase in measured spring-in angle of corner sections manufactured on male tools and a decrease in female tools. It is not clear if the tool-part interaction has an effect on the spring-in of the curved section, or if the measured difference is due to arm bowing in the flat sections.

Another shear process occurring during manufacturing of composite parts is the slippage of the prepreg layers with respect to each other. This mechanism, which has to date received little research attention, is effective in manufacturing parts with corner sections. As the preform for the corner section is imperfect as laid-up, consolidation of the corner under autoclave pressure involves slippage of the prepregs with respect to each other, causing tensile stresses in the tows close to the inner radius, if the prepregs do not slip fully. These stresses are locked in as the part cures, contributing to the increase of the spring-in angle (Fig. 2).

Since tool correction by trial and error is an expensive and time consuming task, the development of an analytical tool to predict the spring-in taking into account various factors has also attracted a considerable research effort, and tool-part interaction is also included in most process models as a major contributor to the final shape of the parts [7-10]. In these models, tool-part interaction is either modelled as the part stuck to the tool surface with no relative motion [8], or as a cure hardening elastic

shear layer which remains intact until the tool is removed [7,9,10]. By adjusting the properties of this shear layer, the amount of stress transferred between the tool and the part can be tailored. With the use of experimental data the shear layer properties were calibrated to an appropriate value. These simulations are based on semi-empirical models, which need to be calibrated according to geometrical deformations observed in manufactured parts.

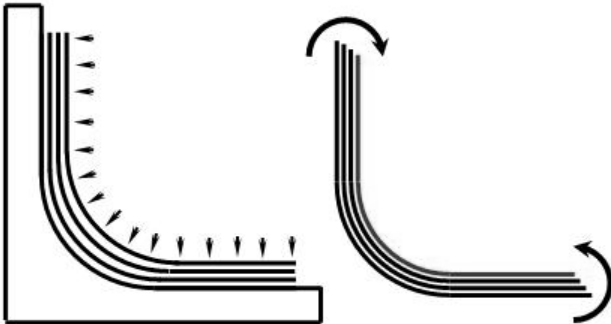


Fig. 2. Fibre stresses due to corner consolidation

Some recent studies concentrate on measuring the tool-part interaction using an instrumented tool. In [11] the researchers have developed a quantitative means of examining the interactions between the tool and the part by applying a strain gauge rosette on a thin aluminium tool and curing a composite part on that instrumented tool under vacuum. This methodology was later used to predict the warpage of flat laminates [12, 13].

A more direct approach was adopted by Kim and Daniel [14] by measuring the strains in the composite laminates during curing using embedded fibre optic strain sensors and electrical resistance strain gauges. Recently Potter et al. [15] used a spot curing technique, where the strain gauges are bonded to cured spots on the prepreg, calibrated in a tensile test machine for load vs. strain. The prepreg is then cured under the MRCC, and the strains recorded.

Flanagan [16] measured the friction coefficients between the Fiberite Epoxy 934 prepreg and the tool surfaces treated by Freekote release agent with or without release film as a function of temperature and pressure. He used a heated plate, and dead weights to simulate the cure cycle, however, the maximum pressure he attained by this method is only a fraction of the autoclave pressure.

The tool-part interaction stresses were measured previously by Ersoy [18]. It has been found that the shear stresses between the prepreg/prepreg interfaces are higher than the shear stresses between the tool-prepreg interfaces for

AS4/8552 composite. Fibre intermingling at the prepreg/prepreg interfaces is believed to cause higher shear stresses as compared to the fibre friction at the tool/part interfaces.

All the previous experimental data show that there is a sliding friction condition at the tool-part interface during the heat up ramps in a MRCC. Another common conclusion that can be drawn from previous studies is that in the early stages of the cure, significant fibre stresses can develop due to friction between the fibre tows and the tool.

In this study a model that takes into account the observations on the interactions between the tool and the part and between the prepreg layers themselves has been developed, and a numerical work has been carried out to investigate the effect of various process parameters and interface properties on the manufacturing distortions of composite parts.

## 2 Finite Element Method

### 2.1 Material Properties

The prepreg investigated in this study is a unidirectional carbon/epoxy, produced by Hexcel Composites with a designation of AS4/8552. The nominal thickness of the prepreg was given as 0.250 mm. The MRCC consists of a first ramp of 2oC/min up to 120 oC and a first hold at 120 oC for 60 min, a second ramp of 2oC/min up to 180 oC and a second hold at 180 oC for 120 min. A pressure of 0.7 MPa is applied throughout the cycle.

During an actual autoclave process, firstly the material is in the viscous state. The composite cannot sustain any transverse stress, whereas it can sustain some fibre stresses. Although the shear modulus of the resin is practically zero, due to fibre friction the shear stresses arising from tool interaction or interply slip can be transferred in the through-the-thickness direction. The autoclave pressure is applied, the rigid mould, which may also impose tool interaction forces, supports the composite. Consolidation takes place as the voids are suppressed, expelled from the composite, and extra resin bleeds.

Then, the resin goes through the rubbery state, defined by a characteristic value of the rubbery modulus of the resin. The cure shrinkage takes place at this step.

Finally, the resin vitrifies and transforms to the glassy state, and resin modulus increases a few orders of magnitude. The deformations imposed in the rubbery state are frozen in and as the autoclave pressure and restraints imposed by the mould are

removed by removing the boundary conditions, the part is allowed to deform freely as it cools down to room temperature.

These considerations suggest that the process should be modelled in three steps: viscous, rubbery, and glassy. The analysis is based on a number of simplifying assumptions, most of which are reasonable. Vitrification is treated as a point at which the material suddenly changes from the rubbery to glassy state with constant properties in each case. To treat this with full viscoelasticity would greatly increase the complexity of the analysis and the amount of material data required, which is difficult to obtain. Assuming fully relaxed properties until an appropriately chosen vitrification point is a pragmatic approach and is argued to be a valid simplification.

In a previous study [19] the properties of AS4/8552 composite in the rubbery and glassy states were obtained by using a Finite Element Analysis based micromechanics approach. The rubbery and glassy properties are given in Table 1. Since there is no data regarding the viscous state, rubbery properties are used in this state.

Table 1 Composite material properties in the rubbery and glassy state [19]

Property	Unit	Rubbery	Glassy
$E_{11}$	MPa	132000	135000
$E_{22} = E_{33}$	MPa	165	9500
$G_{12} = G_{13}$	MPa	44.3	4900
$G_{23}$	MPa	41.6	4900
$\nu_{12} = \nu_{13}$	-	0.346	0.3
$\nu_{23}$	-	0.982	0.45
$\alpha_{22}$	$10^{-6}/^{\circ}\text{C}$	-	32.6
$\epsilon_{22}^{cure}$	%	0.45	-

## 2.2 Solution Steps

The viscous state is represented in Step-1, rubbery state in Step-2 and glassy state in Step-3 respectively. Although the Finite Element Model is implemented as a 3-Step Model, the material properties used in Step-1 and Step-2 are the same, since there is no data about the viscous properties of the material. However, since it is known that significant fibre stresses develop due to tool-part-part interaction in the viscous state; this state is included into the model as the first state. Initially,

the part is at 331.5° C and the tool is at 20° C. A fictitiously high initial temperature is assigned to the part to account for the 0.45% cure shrinkage in the rubbery state as the part cools from 331.5 to 180° C. There is an autoclave pressure of 0.7 MPa on the bag surface of the part. In Step-3, the tool and part cools down to 20° C so that the part becomes glassy. The applied pressure is removed and the part is separated from the tool and spring-in and warpage develops.

## 2.3 Elements

8-node biquadratic quadrilateral generalized plane strain elements are used. The generalized plane strain theory used in ABAQUS assumes that the model lies between two bounding planes, which may move as rigid bodies with respect to each other, thus causing strain in the direction perpendicular to the plane of the model. It is assumed that the deformation of the model is independent of position with respect to this direction, so the relative motion of the two planes causes a direct strain in the direction perpendicular to the plane of the model only. The elements are defined with a reference node, and restraining this node gives a plane strain condition whereas setting it free gives a plane stress condition.

In the FEA model, a common reference node is defined for both the tool and the part in Step-1 and Step-2. This reference node is restrained for rotation so that the two bounding planes are free to displace but do not rotate with respect to each other. This allows the thermal expansion effect of the tool perpendicular to the plane of the model to be taken into account, and preventing the spread of the composite in viscous or rubbery states under the autoclave pressure. Upon vitrification, the modulus increases and the restraints imposed by the tool cease to be effective. The tool is removed from the model in Step-3, and the part section is now in a plane stress condition. The use of generalized plane strain elements allows one to switch from the plane strain condition in the rubbery state to plane stress in the glassy state by removing the restraints on the reference node common to all elements.

## 2.4 Interface Behaviour

When developing the FEA models, both the tool/part and interply interactions are considered. A similar model was used by Twigg et al [13] which assumed that slip occurs between the plies of the laminate itself in addition to the tool-part interface and for simplicity it is assumed that the sliding friction condition occurs only at two interfaces:

between the tool and the ply adjacent to the tool and between this ply and the rest of the part. Other assumptions are as follows:

- The laminate is uni-directional and hence the modulus and thermal expansion of each ply is identical [13].
- The interply sliding friction coefficient is smaller than the interface sliding friction coefficient. This is based on experimental evidence presented by Flanagan [16].

There are two contact pairs, one of them is between the tool and the ply adjacent to the tool and the other is between the ply adjacent to the tool and the rest of the plies (as a single part). Both contact pairs are active during Step-1 and Step-2, and the tool/part contact is deleted in Step-3, and interply contact is switched to ROUGH in Step-3. Tool/Part and interply interactions are modelled using ABAQUS mechanical contact interaction modelling capabilities. Contact surfaces are defined for interactions, using ABAQUS option \*SURFACE, and then these surfaces are matched by using the option \*CONTACT PAIR. The characteristics of the contacting surfaces are defined by using the option \*SURFACE BEHAVIOR.

Different surface characteristics can be defined by the latter option. Interaction normal to the surface is the default "hard" contact relationship, which allows no penetration of the slave nodes into the master surface and no transfer of tensile stress across the interface. Interaction tangential to the surface is modelled with the classical isotropic Coulomb friction model, where the interfacial shear stress is proportional to the contact pressure, and the constant of proportionality is the friction coefficient. In addition to this, ABAQUS allows the introduction of a shear stress limit, which is the maximum value of shear stress that can be carried by the interface before the surfaces begin to slide (Fig.3).

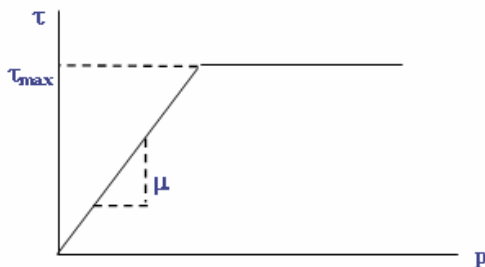


Fig. 3- Interface friction characteristics

Parameters for interfaces used for modelling interply and tool/part interactions are listed in Table-2 below.

Table 2 Interface parameters

<i>Parameter</i>	<i>Definition</i>	<i>Value</i>
$\mu$	Friction coefficient between tool/part	0.5
$\mu$	Friction coefficient between plies	0.3
$\tau_{\max}$	Sliding stress between tool/part	0.2 MPa
$\tau_{\max}$	Sliding stress between plies	0.1 MPa

## 2.5 Geometry

### 2.5.1 Flat Strips

For flat composite strips the model has three parts: the tool, the ply adjacent to the tool and the rest of the part. The part consists of 4-ply with a total thickness of 1 mm. The thermal expansion of the aluminium tool is defined to be  $24.7 \times 10^{-6} \text{ } ^\circ\text{C}^{-1}$  and the elastic modulus is 73 GPa. Only the top nodes of the tool are restrained in the vertical direction, and the symmetry line in the horizontal direction. The geometry and meshing of this model is shown in Fig.4.

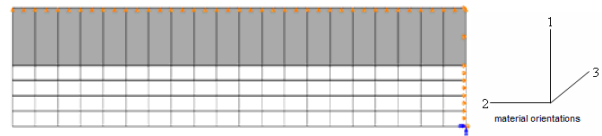


Fig. 4- Meshing of flat part for Model-2

### 2.5.2 C-sections

The mesh geometries for the C-sections are shown in Fig. 5. Only half of the C-sections are modelled by taking advantage of the symmetry. Since the C-sections are made in a composite tool with fibres running in the hoop direction, with no thermal expansion in that direction, tool interaction is assumed to be zero. This allows avoiding modelling of the tool, by just assigning sliding boundary conditions along the hoop direction. The lack of tool-part interaction also allows the manufacturing cycle to be modelled only in two steps: rubbery and glassy. In Step-1 the nodes on the tool side are restrained normal to the tool while sliding along the tool is allowed. The autoclave pressure is modelled as surface pressure on the vacuum bag side.

In Step-2, upon vitrification the modulus increases and the restraints imposed by the tool

cease to be effective, and the section is in plane stress condition.

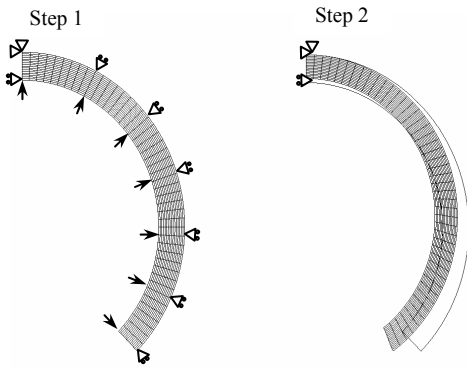


Fig. 5. The Finite Element mesh and the boundary conditions for the C-sections.

### 2.5.3 L-sections

The L-sections of 100 mm arm length and 20 mm radius are made in a female Invar tool. (Fig.6)

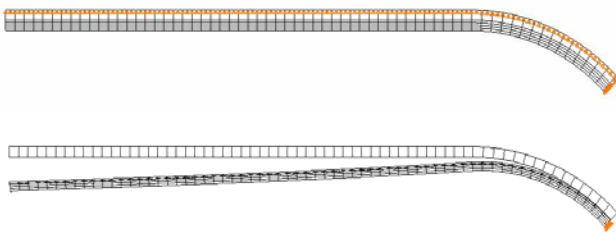


Fig. 6. The Finite Element mesh and the boundary conditions for the L-sections.

As in the flat strips, the tool is included in the model and the part is modelled with a separate ply adjacent to the tool and a common reference node is used for the tool and the part.

The tool material is invar with an elastic modulus of  $148 \times 10^{12}$  MPa and thermal expansion coefficient of  $1.5 \times 10^{-6} \text{ } ^\circ\text{C}^{-1}$ . Since the mould is not modelled to its full thickness, an artificially higher modulus is used to compensate for tool deformation.

In the Finite Element Method three steps are defined but as in the flat parts, the material properties used in Step-1 and Step-2 are the same, since there is no data about the viscous properties of the material.

## 3 Results and Discussion

### 3.1 Flat Strips

The shear stress and fibre direction stress distributions across the thickness of the unidirectional flat strip are shown in Fig. 7 and Fig.

8 respectively. The shear stress distribution is the same along all cross sections except a very short distance from the symmetry line. There are two observations to be made: Firstly, the shear stress distribution is bi-linear with a value of 0.1 MPa at the interply interface and 0.2 MPa at the tool-part interface. These values are the maximum shear stresses that these interfaces can carry. Secondly, there is a discontinuity in fibre stresses at the interface between the ply adjacent to the tool and the rest of the plies. The fibre stress distributions cause a net bending moment which gives the curvature of the strip when it is released from the tool.

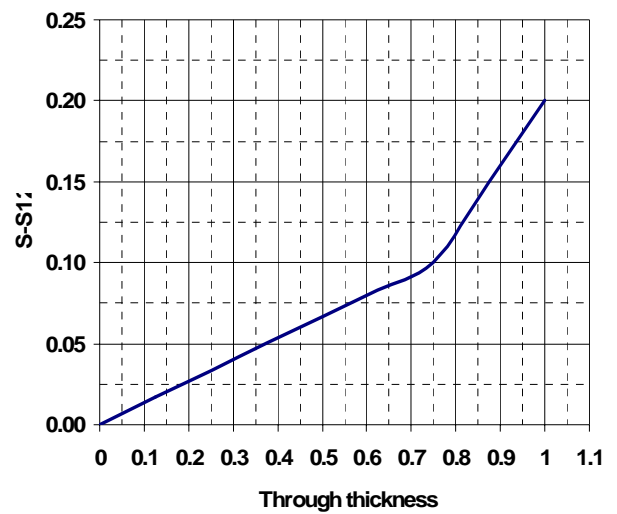


Fig. 7.  $S_{12}$  values for 500mm long part at the end of Step-2 (MPa)

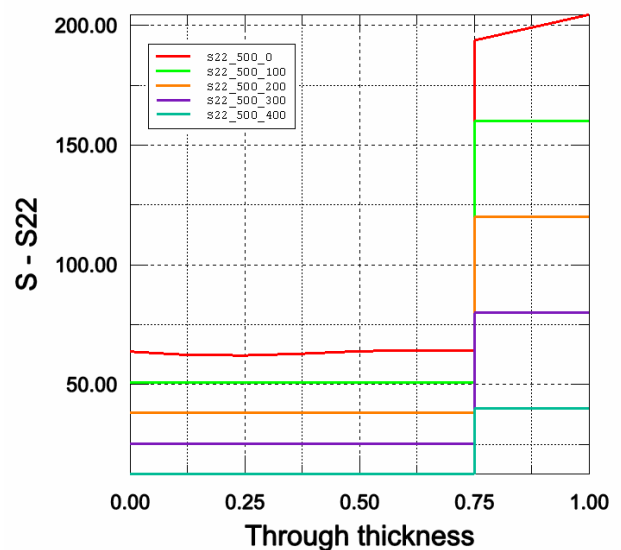


Fig. 8. The fibre direction stresses at various cross sections (0, 100, 200, 300, and 400 mm away from the symmetry line) at the end of Step-2 (MPa)

In Figs. 9 and 10, the contact pressure (CPRESS), contact opening (COPEN), contact shear stress (CSHEAR) and relative slipping (CLIP) at the tool-part interface and at the interface between the ply adjacent to the tool and the rest of the part are plotted. Contact shear stress remains almost constant along the length of the part in both interfaces except a very short distance from the symmetry line, implying that sliding condition prevails. There is a only in a small region close to the symmetry line of the part where the interfaces are sticking.

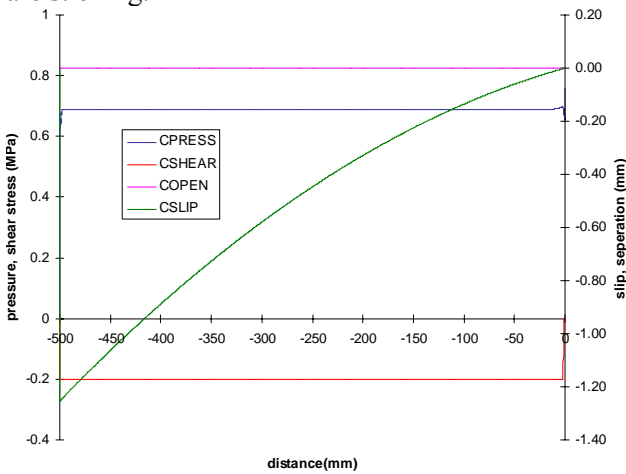


Fig. 9. Interface stresses and displacement contact outputs between tool and part at the end of Step 1.

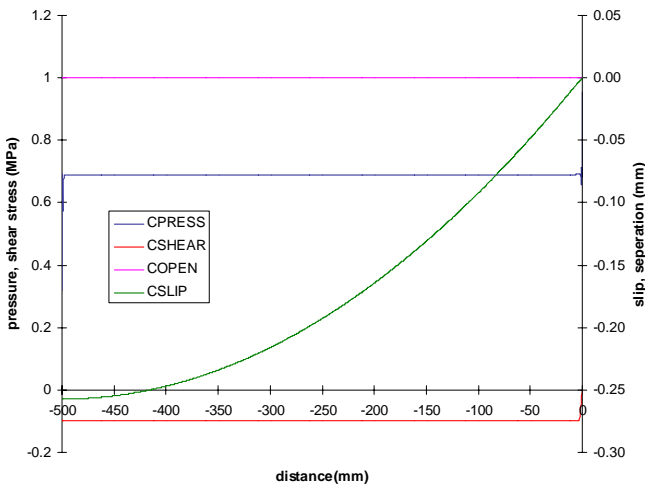


Fig. 10. Interface stresses and displacement contact outputs between ply adjacent to the part and the rest of the plies at the end of Step 1.

### 3.2 C-sections

Spring-in values predicted by the FEA and measured for different thicknesses are given in Fig. 11 for unidirectional (UD) C-sections manufactured inside a tube made of the same material and the

fibres running in the hoop direction [20]. This plot shows a considerable decrease in spring-in with part thickness increasing from 1 to 4 mm. The thermoelastic component is  $0.47^\circ$ , and so the non-thermoelastic component of spring-in, as calculated in the FEA is decreasing by a factor of more than 2 over this range. This confirms that thickness does have a substantial effect on spring-in, as predicted by the shear-lag theory proposed in another study carried out by the authors [21].

The correlation with experimental results is good. The measured trend of decreasing spring-in with increasing thickness matches well the trend predicted from the analytical solution proposed by the authors [21]. Experimental spring-in angles are very close to those predicted for the thicker parts, and slightly lower for the thinner ones, with a maximum difference of 15%, which is reasonable given the difficulty of measuring shrinkage accurately, and uncertainty over the rubbery shear modulus which was a calculated rather than measured value.

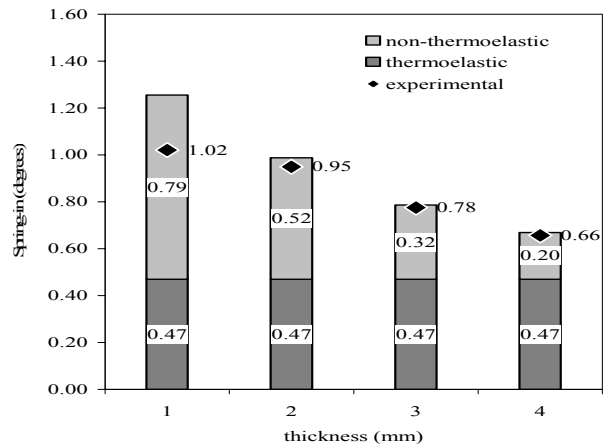


Fig. 11-. Predicted and measured spring-in values for unidirectional parts.

Fig. 12 shows the stress distribution at the end of the first and second steps along the symmetry plane in the unidirectional C-section parts of 4 mm and 2 mm thickness. It can be seen that the fibre stresses can reach up to 50 MPa tensile on the tool side, and -50MPa on the bag side for both the 4 mm and 2 mm thick parts. The analysis performed by reapplying the autoclave pressure on the bag side showed that the part remains in contact with the tool after vitrification and before cool down. The stresses are rearranged when the part is removed from the tool and cooled down, and the maximum residual stress at the end of Step 2 is 15 MPa for the 4 mm thick part, and 3.6 MPa for the 2 mm part.

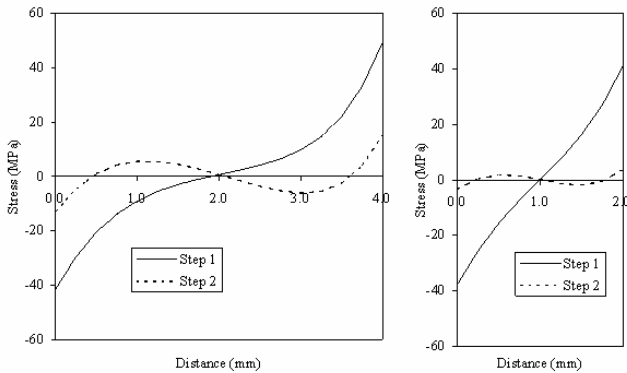


Fig. 12. Hoop direction stresses along the thickness of unidirectional C-section parts of two different thicknesses.

### 3.3 L-sections

#### 3.3.1 Through-the-thickness deformation

In Fig. 13, the through-the-thickness strain is plotted along the length of the L-sections of 1, 2, 3, and 4 mm thick, at the end of the process. The final through-the-thickness strain in the arms of specimens are relatively constant, and at the corner, consolidation is less for thicker specimens, resulting in “corner thickening” due to lack of consolidation. Fig. 14 shows the general pattern of the deformation. At Step-2, the compaction is basically in the arms, whereas the corner consolidation strains are much less than the arm consolidation strain. The shear deformation due to consolidation can be observed from the deformed mesh. Cure shrinkage causes the corner region to loose contact with the tool. At Step-3, the deformations occurring at Step-2 are locked in as the part separates from the tool. This phenomenon can be observed as a resin rich layer in the corner sections manufactured on female tools.

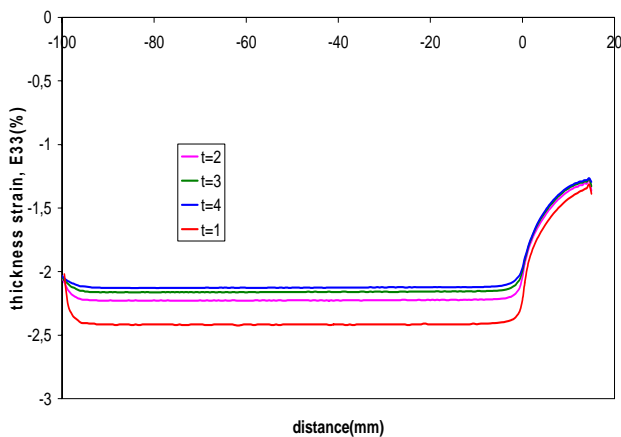


Fig. 13. Effect of thickness on final through-the-thickness strains

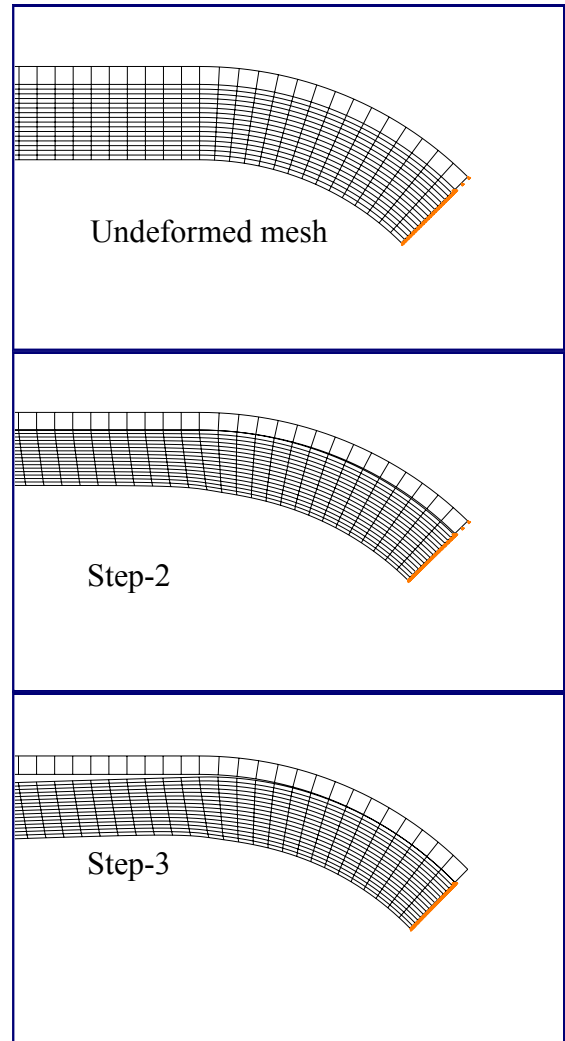


Fig. 14. Deformation of the mesh at the corner

#### 3.3.2 Interface Behaviour

The interface stresses between the tool and the part cause internal stresses during the first two steps where the tool is expanding. These stresses are locked in as the part vitrifies, and cause deformation of the part to conform to its final shape after the part is released from the tool and cools down.

In Fig.15 the contact pressure (CPRESS), contact shear stress (CSHEAR), contact opening (COPEN), and relative slipping between the tool and the part (CSLIP) are shown at the end of Step1. There is a slight opening at the corner. Shear stress linearly decreases to zero towards the corner.

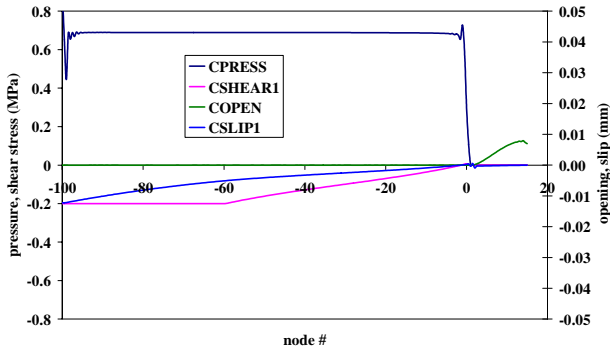


Fig. 15. Interface stresses and displacements for 1mm thickness at the end of Step-2

### 3.3.3 Spring-in

The total spring-in is found by calculating the angle between the positions of the arm at the beginning and at the end of the process, where the corner spring-in is twice the angle between the tangents passing from the symmetry line of the corner at the beginning and at the end of the process. These angles are shown in Fig. 16.

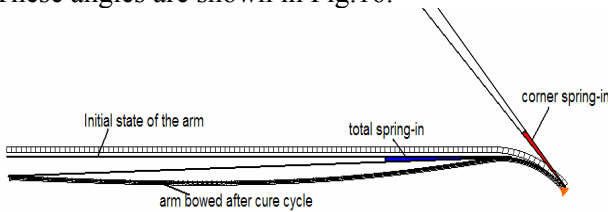


Fig. 16. Total spring in and corner spring-in

In Fig. 17, experimental and numerical values of total spring-in angle are compared for 0.5, 1 and 2 mm thick parts manufactured in a female invar tool. The total spring-in in the 0.5 mm part is negative, which means that this part actually springs out. The model cannot capture this phenomenon, and it is believed this is due to the lack of reliable data about the interface frictional stresses.

### 3.3.4 Arm bowing

Arm bowing is a well known phenomenon observed in L-sections, and in relatively thin sections, the arm bows convex from the tool. The arm bowing of the parts modelled is found to be dependent on the thickness. In Fig. 18, the sense of arm bowing is correct, since the model predicts the arms bowing convex from the tool as observed and the amount of bowing decreases with increasing thickness.

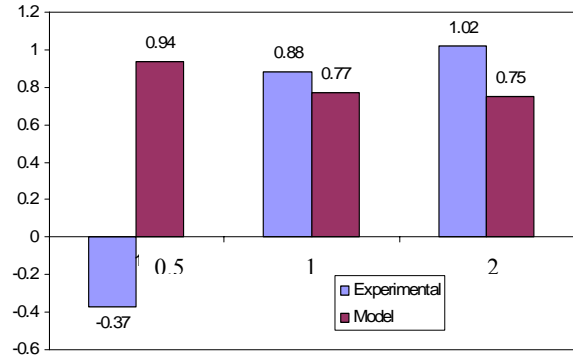


Fig. 17. Experimental and numerical values of total spring-in for parts of different thickness are compared

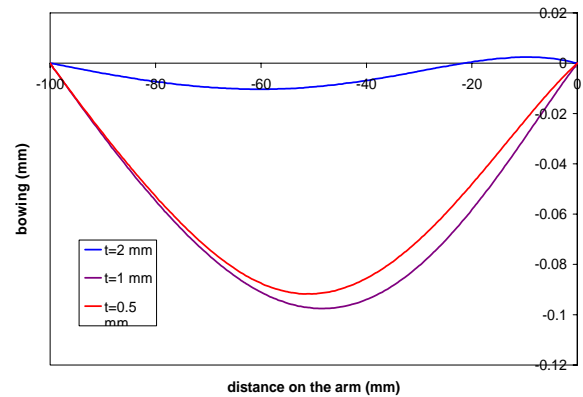


Fig. 18. Arm bowing for parts of different thickness at the end of Step-3

### 3.3.5 Stresses across the thickness

Various cross sections where the stresses are plotted as well as the coordinates in which the stresses are defined are shown in Fig. 19. These cross-sections are at 45° (symmetry line), and 67.5° on the curved section, and at 0 mm and 50 mm on the flat section. In Fig. 20,  $S_{22}$  stress values are plotted across the thickness at various cross sections. At the cross-section in the middle of the flat part (50mm),  $S_{22}$  values are almost constant with a discontinuity at the interface between the ply adjacent to the tool and the rest of the ply. This trend was similar to the one observed previously in the flat composite strips. However, in the curved section of the L-sections the behaviour is completely different, because of fibre consolidation in these regions. As the resin shrinks the fibres at the inner radius are forced to move towards the outer radius, which puts the fibres in tension. This stress decreases towards the outer radius. There is a discontinuity in stress because of the interply interface. The model predicts compressive stresses towards the tool side; however

the fibres are not supposed to carry compression in the viscous and rubbery states since they may buckle. This is an insufficiency of the model which will be considered in future work.

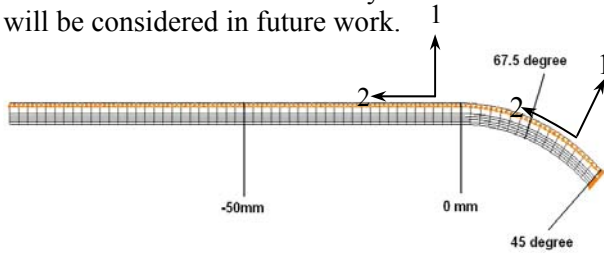


Fig. 19. Cross sections for 100 mm long part.

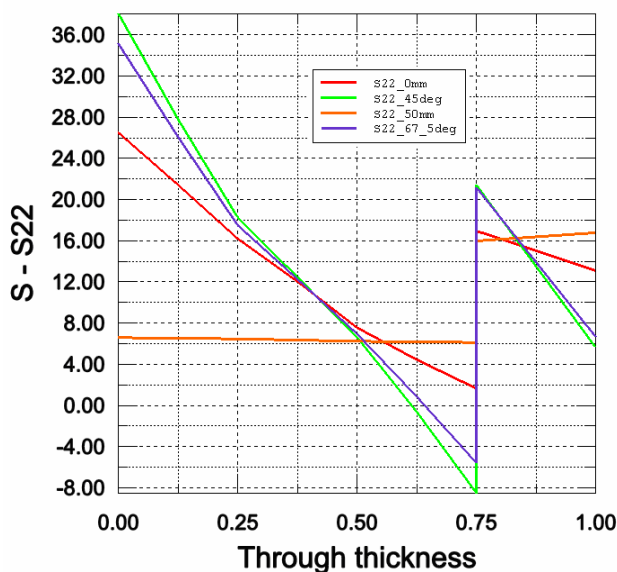


Fig. 20.  $S_{22}$  values at the end of Step-2

#### 4 Conclusions

In this study, shape distortions and stress distributions in flat strips, C- and L-sections are investigated.

In flat parts, the warpage depends greatly on the magnitude of the maximum interply shear stress and maximum tool/part shear stress. There is a discontinuity in fibre stresses at the interply interface, causing a bending moment, explaining the curvatures obtained in flat strips.

The spring-in angles of C-sections are predicted successfully using a two step finite element analysis procedure. A specimen geometry and manufacturing process was designed to leave the consolidation and tool part interaction out and in order to measure the intrinsic spring-in angles of corner sections of various thicknesses and lay-ups.

In L-sections, the model captures most of the shape distortions observed in real parts: corner thickening, arm bowing, and corner spring-in.

The analysis is based on a number of simplifying assumptions, most of which are reasonable. Vitrification is treated as a point at which the material suddenly changes from the rubbery to glassy state with constant properties in each case. Although the Finite Element Model is implemented as a 3-Step Model, the material properties used in Step-1 and Step-2 are the same, since there is no data about the viscous properties of the material. However, since it is known that significant fibre stresses develop due to tool-part-part interaction in the viscous state; this state is included in the model as the first state.

For the rubbery and glassy states of the part, 18 material properties are defined in the models. From these properties, the modulus in the transverse direction  $E_{22}$ , shear moduli  $G_{12}$  and  $G_{23}$  have the most dominant role in modelling the deformation behaviour of the composite part, because they can affect the residual stresses generated during the cure cycle. Also, in modelling the frictional behaviour between two surfaces, assumed values for the maximum shear stress,  $\tau_{max}$  are used. It is shown that the warpage depends greatly on the magnitude of the maximum interply shear stress. To have a more correct model representation, these parameters should be measured.

#### 5 Acknowledgements

This research is supported by Bogazici University Research Fund (Project Code: 07A606), and by University of Bristol as a sponsored thesis.

#### 6 References

- [1] Pagliuso, S., Warpage, "A nightmare for composite parts producers", in: Hayashi, T., Kawata, K., Umekawa S., editors. *Progress in Science and Engineering of Composites, ICCM 4*, p. 1617-23, 1982.
- [2] Radford, W. D., "Cure shrinkage induced warpage in flat uni-axial composite", *Journal of Composite Technology and Research*, Vol. 15, No. 4, pp.290-296, 1983.
- [3] Cann, M. T., and Adams, D. O., "Effect of part-tool interaction on the cure distortion of flat composite laminates", *46<sup>th</sup> International SAMPE Symposium*, May 6-10 2001.
- [4] Radford, D.W. and Rennick, T.S., "Separating sources of manufacturing distortion in laminated

- composites”, *Journal of Reinforced Plastics and Composites*, 19(8):621–641, 2000.
- [5] Darrow, D. A. Jr., Smith, L. V., “Isolating components of processing induced warpage in laminated composites”, *Journal of Composite Materials*, Vol. 36, No. 21, 2002.
- [6] Albert C. and Fernlund G., “Spring-in and warpage of angled composite laminates”, *Composites Science and Technology*, 62: 1895–1912, 2002.
- [7] Ferlund, G., Rahman, N., Courdji, R., Bresslauer, M., Poursartip, A., Willden, K., Nelson, K., “Experimental and numerical study of the effect of cure cycle, tool surface, geometry, and lay-up on the dimensional fidelity of autoclave-processed composite parts”. *Composites: Part A*, 33:341-351, 2002.
- [8] Zhu, Q., Geubelle, P. H., Li, M. Tucker C. L. III, “Dimensional accuracy of thermoset composites: simulation of process-induced residual stresses”, *Journal of Composite Materials*, 35(24): 2171-2205, 2001.
- [9] Johnston, A. “*An integrated model of the development of process-induced deformation in autoclave processing of composites structures*”, Ph.D. Thesis, The University of British Columbia, Vancouver, 1997.
- [10] Johnston, A. Vaziri, R., and Poursartip, A. “A plane strain model for process-induced deformation of laminated composite structures”, *Journal of Composite Materials*, 35(16): 1435-1469, 2001.
- [11] Twigg, G., Poursartip, A., and Fernlund, G., “An experimental method for quantifying tool–part shear interaction during composites processing”, *Composites Science and Technology*, 63, 1985–2002, 2003.
- [12] Twigg, G., Poursartip, A., and Fernlund, G., “Tool-part interaction in composites processing. Part II: Numerical modelling”, *Composites: Part A*, 34 (11), 2003.
- [13] Twigg, G., Poursartip, A., and Fernlund, G., “Tool-part interaction in composites processing. Part I: Experimental investigation and analytical model”, *Composites: Part A*, 34 (11), 2003.
- [14] Kim, Y. K., and Daniel, I. M., “Cure cycle effect on composite structures manufactured by resin transfer molding”, *Journal of Composite Materials*, Vol. 36, No. 14, 2002.
- [15] Potter K. Campbell M & Wisnom MR, “Investigation of tool/part interaction effects in the manufacture of composite components”, *Proceedings of ICCM-14, 14th International Conference on Composite Materials*, San Diego, USA, 14-18 June 2003.
- [16] Flanagan R. “*The dimensional stability of composite laminates and structures*”, PhD Thesis, Queen’s University of Belfast; 1997.
- [17] Martin, C.J, Seferis, J.C., and Wilhelm M.A., “Frictional resistance of thermoset prepregs and its influence on honeycomb composite processing”, *Composites: Part A*, 27A, pp. 943-951,1996.
- [18] Ersoy N., Potter K., Wisnom M. R., Clegg M. J., “An experimental method to study the frictional processes during composites manufacturing” *Composites: Part A*, 36, 1536–1544, 2005.
- [19] Ersoy N., Garstka T., Potter K., Wisnom M. R. and Clegg M., “Micromechanical models to predict and tests to measure the development of AS4/8552 composite properties through cure”, to be published.
- [20] Ersoy N., Potter K., Wisnom M. R., “Modelling of the spring-in phenomenon in curved parts made of AS4/8552 composite”, to be published.
- [21] Wisnom M.R., Ersoy N. Potter K.D., “Shear-Lag Analysis of the Effect of Thickness on Spring-in of Curved Composites”, *Journal of Composites Materials*, in press.